· Florida · **Tallahassee**

· Upper Austria · **Wels**

Insulation System Reliability in Hybrid AC/DC Electrical Assets: The Space Charge Issue

submitted as a Research Report for the Marshall Foundation

2022

Autors

Thomas Pichler, B.Sc.

Study Program

Electrical Engineering

Supervisor

FH-Prof. DI Dr.techn. Priv.Doz. Sumereder

Prof. Dr. Gian Carlo Montanari

Date

10.10.2022

Stelzhamerstraße 23
A-4600 Wels, Austria

www.fh-wels.at

Abstract

In 1985 Takada developed a acoustic based method to evaluated polarization and injected electric charges in Dielectrics. This method is known since then, but is still not really common in the evaluation of insulation materials. For the monitoring of insulation material under AC voltage, the partial discharge measurement and the dissipation factor measurement have clearly prevailed. For the evaluation of DC insulation systems, however, it is somewhat more difficult, since the phase relationship between the current and voltage is lost. Therefore Space Charge measurement might become more important in the near future, to evaluate the degradation of insulation material. Moreover, the effect of charge injection cannot be detected with a partial discharge equipment.

The results of the space charge measurement show quite different results for the different materials as well as for the different applied electrical field magnitudes. Very interesting is the difference of charge accumulation at the electrodes, where Kapton accumulates hetero charge, but Fluorinated Ethylene Propylene accumulates homo charge there. The charge carrier stored in the bulk, due to the effects of polarization and charge carriers injected, appear to be very different for the two materials as a function of electrical field. While the accumulated charge has a rather linear course for Kapton, the same effects take a rather exponential course for Fluorinated Ethylene Propylene and has a threshold level in terms of the magnitude of the electric field.

Table of Contents

1 Introduction

In the course of time, great progress has been made in power electronics in recent years. The components developed in this process are becoming increasingly powerful and voltage-resistant. For this reason, power electronics is becoming more and more important in high-voltage engineering. This opens up a new, old-well known possibility for electrical power distribution to implement Thomas Alva Edison's initially preferred method of power distribution by means of Direct Current(=DC). The reduction of the effects of reactive power components and skin effect, as well as the higher transmitted power per volume are only a few advantages that would speak for a change from AC to DC. [1] The key technology in this context is power electronics in order to vary the desired voltage levels, since transformers cannot be used under DC. However, when DC voltage is used by means of DCDC converters, a superimposed ripple occurs due to the fast switching frequencies. This prevents a complete disappearance of the first two mentioned effects. [2]

The change of the network distribution voltage form from AC to DC voltage with superimposed ripple does not only mean the use of power electronics, but also leads to a changed in stress onto the insulation system. Transient switching operations in distribution networks lead to voltage peaks. [3] [4] The electric field distribution during these switching transients is therefore similar to the electric field under AC. From this follows the insulation system needs to be capable for AC and DC. However, the insulation is exposed to the DC voltage for most of the time. While under AC the dielectric constant is responsible for the electric field distribution with layered dielectric, the electric field distribution with DC results from the different conductivities of the materials. [1] [5] This would not be a problem if both parameters behave the same or remain constant in case of an external influence. However, this is not the case, while the dielectric constant changes only marginally with different weather and temperature variations, this affects the conductivity of the insulation materials very strongly. The fluctuations under AC for the dielectric constant are in the tens, but for the conductivity, fluctuations can go far beyond several powers of ten. [6] [4]

The evaluation of insulation materials under AC for its degradation, is mostly investigated with partial discharge detectors. This method has been performed for decades and, with the dissipation factor measurement, it is the most commonly used method to find out the degree of degradation. [7]

At the present time, no method has become widely accepted for testing insulation materials under DC voltage. Partial discharge measurement is also used for DC voltage. However, the phase reference of current and voltage is lost. In addition, PD pulses occur much less frequently due to the high time constant. [4] [7] [5] Therefore, mirroring the

evaluation methods from AC to DC makes it difficult to detect PD pulses, especially in noisy environment. This does not mean that the partial discharge measurement under DC does not make sense. However, it makes the evaluation of PD under DC very difficult at the moment. [7]

The above arguments lead scientists and the industry to find other ways to test insulation systems for degradation. In 1985, Takada introduced an acoustic method to determine the amount of space charge density in insulation materials. The lack of market from testing insulation systems under DC stress has made this measurement system somewhat forgotten. As the trend in electrical energy transmission is moving back towards DC voltage transmission due to the arguments mentioned above, this measurement system is more up-to-date than ever. In addition, the development of high-voltage insulation is moving towards ever higher nominal electric field strengths. At very high electric field strengths of over 100kV/mm at room temperature, charge injections can occur at the electrodes into the insulation material, which can only be represented and differentiated from other effects such as occurring partial discharge on the basis of the space charge measurement. [8] [9]
In this further report, space charge measurements using the Pulsed Electro Acoustic method were performed on Kapton (Polyimide-Film) and Fluorinated Ethylene Propylene (=FEP).

2 Direct Current at a Polymer based Insulator

If voltage is applied to an insulating material, different polarization processes first occur within the bulk of the insulator, depending on the frequency of the voltage. As the frequency of the applied voltage approaches zero, further polarization processes occur, which do not occur with an AC voltage with a nominal frequency of $\mathbf{50}\ \boldsymbol{Hz}$. Due to the decay and almost complete disappearance of the polarization current, the field distribution changes and goes from a capacitive to a resistive field distribution. This results in charge accumulation at the interfaces of different conductivities. The accumulation of charge carriers at the material interfaces in the insulator influences the initial electric field resulting from the charge accumulation at the electrode surfaces. [10] The specific conductivity of polymer-based insulating materials depends on different mechanisms, therefore an integral current measurement (PD-measurement) does not provide information about the processes taking place as well as about the nature of the charge carriers involved. [11] It is also important to clarify the injection of charge into the insulating material. This requires a spatial and chronological resolution of space charge in the solid insulating material. For this purpose, the Pulsed Electro Acoustic, the pressure wave method and the thermal step method have become widely used.
As already mentioned, the conductivity depends on many factors. The criteria that influence the conductivity the most are the electric field strength [12] [13], the temperature [14] [13], the humidity [15] and the time [13]. However, in order to gain a deeper understanding of the transport of charge in polymer-based insulating materials under DC voltage, the change in the cause of electrical conductivity must be considered in more detail. The different processes that occur make it difficult to create a single charge transport model as known from semiconductor technology.

3 Pulsed Electro-Acoustic Method

The Pulsed Electro Acoustic (=PEA) method was developed by Takada, as already mentioned. The principle of this method is based on Coulomb's one-dimensional force law. The basic operating principle is shown in ***Fig.* 1**. It consists of a High voltage DC-Generator, which is responsible for the constant high electric field over time within the sample and allow the accumulation of space charges. [16] The High DC voltage applied to the sample is superimposed with a pulse voltage $\boldsymbol{e_p(t)}$, which has a short on time and a defined frequency in the low kHz range. The pulse will move the accumulated charge carriers slightly, this movement by the charge carriers generates an acoustic wave which travels through the sample and the ground electrode and is then recorded with a piezo electric sensor. This sensor allows the conversion from an acoustic signal to a voltage signal proportional to the space charges. The absorber after the piezo-sensor is used to

avoid reflections of the acoustic signal. The amplifier after the piezo electric sensor keeps the signal-to-noise ratio as big as possible, since the output voltage of the piezo electric sensor is very low. The amplified voltage signal is then recorded with the scope and sent to a computer to be first saved and then post processed. [16] [17] [18]
***Equ*.3.1** shows the mathematical expression for the output signal in the frequency domain.

$$V(f) = S(f)[\frac{\sigma(0)}{v_s \Delta\tau} + R(f) + \frac{\sigma(d)}{v_s \Delta\tau} exp(-\frac{ifd2\pi}{v_s})] \tag{3.1}$$

- $\boldsymbol{S(f)}$ System response function that depends on the transducer and the amplifier
- $\frac{\sigma(0)}{v_s \Delta\tau}$ Surface charge at the ground electrode
- $\boldsymbol{R(f)}$ accumulated charge in the sample
- $\frac{\sigma(d)}{v_s \Delta\tau} \boldsymbol{exp}(-\frac{ifd2\pi}{v_s})$ surface charge at the high voltage electrode
- $\boldsymbol{Delta\tau}$ sampling time
- $\boldsymbol{v_s}$ speed of sound
- $\boldsymbol{d}$ sample thickness

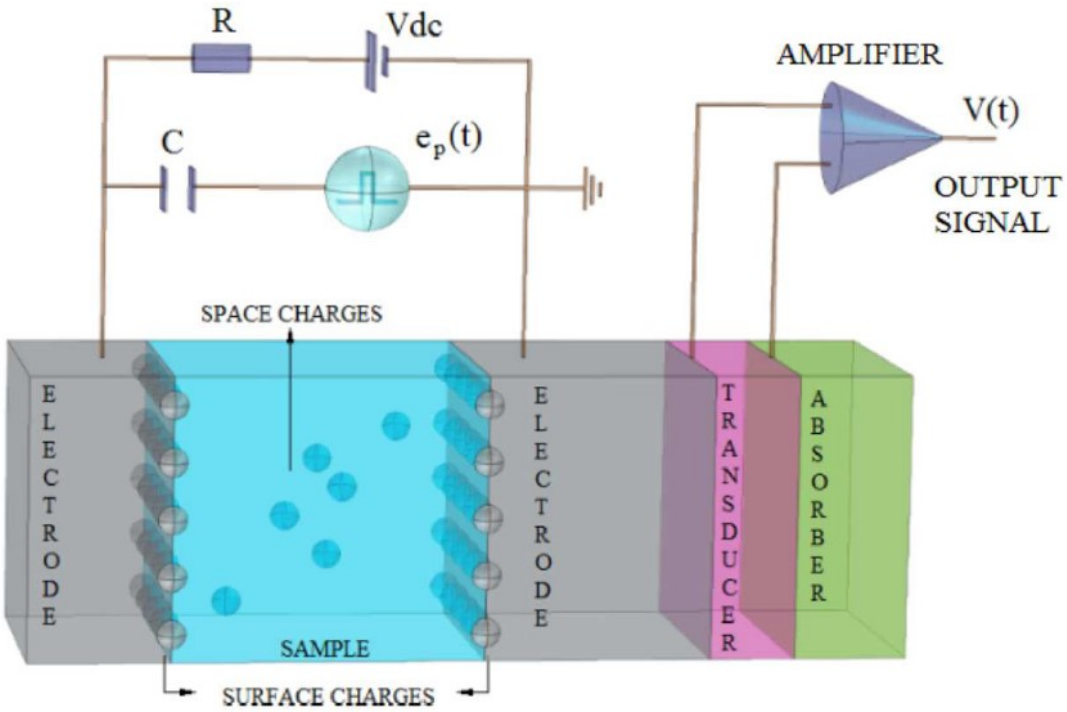

Figure 1: Measurement and function principle of the PEA-method
source: [16]

3.1 Generated and Induced Surface Charges

If ***Fig.* 1** is used as an illustration and a voltage is applied to the test specimen, the charge initially accumulates on the surface of the material with the lowest conductivity. The accumulated charge then depends on the electric field $\boldsymbol{E_{dc}}$ and on the permittivity of the material $\boldsymbol{\varepsilon}$. [16]

$$\varepsilon = \varepsilon_0 \varepsilon_r \tag{3.2}$$

$$E_{DC} = V_{dc}/d \tag{3.3}$$

$$\sigma_{DC} = \varepsilon E_{dc} \tag{3.4}$$

Where:

- $\boldsymbol{\varepsilon_0}$ permittivity of free space
- $\boldsymbol{\varepsilon_r}$ relative permittivity of the material
- $\boldsymbol{d}$ thickness of the specimen
- $\boldsymbol{V_{dc}}$ applied voltage

The calculation of ***Equ.* 3.3** refers to a uniform electric field, where fringing fields at the edges of the electrodes are neglected. [19]

The accumulated surface charges at the high voltage electrode and at the Ground electrode are of the same magnitude, but opposite in sign. [16]

$$\sigma_{dc}^{+} = \varepsilon E_{dc} \tag{3.5}$$

$$\sigma_{dc}^{-} = -\varepsilon E_{dc} \tag{3.6}$$

Assuming a positive voltage, the positive charges accumulate at the interface between the high-voltage electrode (Anode) and the test specimen. The negative charges accumulate at the interface between the ground electrode (Cathode) and the test specimen. The superscripts in ***Equ.* 3.5** and ***Equ.* 3.6** illustrate this. Similarly, the superimposed pulse voltage, which is responsible for the movement of the charge, generates additional surface charge.

As with the surface charge from the applied DC voltage, this occurs on both electrodes with different signs. [16]

$$\sigma^{+}_{pulse} = \frac{\varepsilon}{2} e_p(t) \tag{3.7}$$

$$\sigma^{-}_{pulse} = -\frac{\varepsilon}{2} E_p(t) \tag{3.8}$$

As soon as space charge $\boldsymbol{\rho(x)}$ accumulates in the bulk of the material, injected by the surface charge, the surface charge results in opposite magnitude, but with the same sign. The ratio in front shows the injection of the space charge starting from the high voltage electrode (***Equ.* 3.9**) or from the Ground electrode (***Equ.* 3.10**), respectively. [16]

$$\sigma^{+}_{p} = -\int_{0}^{d} \frac{x_p}{d} \rho(x) dx \tag{3.9}$$

$$\sigma^{-}_{p} = -\int_{0}^{d} \frac{d - x_p}{d} \rho(x) dx \tag{3.10}$$

The total surface charge for the High voltage electrode and the Ground electrode results then in the following Equations: [18]

$$\sigma^{+} = \sigma^{+}_{dc} + \sigma^{+}_{pulse} + \sigma^{+}_{p} = \varepsilon E_{dc} + \frac{\varepsilon}{2} e_p(t) - \int_{0}^{d} \frac{x_p}{d} \rho(x) dx \tag{3.11}$$

$$\sigma^{-} = \sigma^{-}_{dc} + \sigma^{-}_{pulse} + \sigma^{-}_{p} = -\varepsilon E_{dc} - \frac{\varepsilon}{2} e_p(t) - \int_{0}^{d} \frac{d - x_p}{d} \rho(x) dx \tag{3.12}$$

Since the magnitude of the generated field strength caused by the pulse voltage $\boldsymbol{(e_p(t))}$ is only a minor part of the magnitude of the electric field strength caused by the high voltage source $\boldsymbol{(E_{dc})}$, this term can be neglected from the equation. [18] [16]

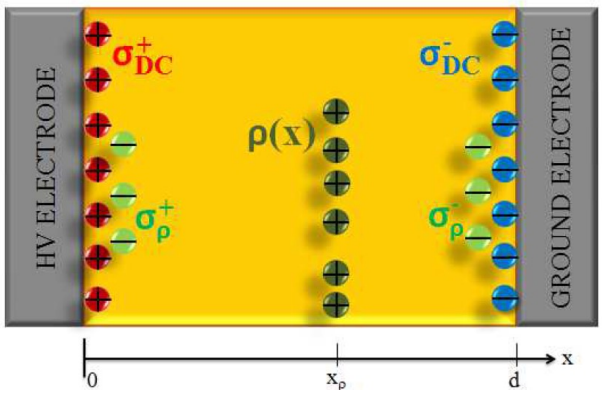

Figure 2: accumulated surface charges at the interfaces of the electrode caused by the applied electric field $\boldsymbol{E_{dc}}$ as well as injected space charges $\boldsymbol{\rho(x)}$ source: [16]

3.2 Electrostatic Forces

As explained at the beginning of this chapter, the working principle of this measurement is based on the one-dimensional Coulomb's law of forces. The accumulated charge on both electrode surfaces strives for a charge exchange until a charge equilibrium is established, which is prevented by the low conductivity of the test specimen. The accumulated charge due to the high electric field is exposed to the total electric field from the sum of the DC voltage source and the pulse generator. [16]

$$E(x,t) = E_{dc}(x) + e_p(t) \tag{3.13}$$

The mathematical description formulated by Coulomb law of force is:

$$F = qE \tag{3.14}$$

- $\boldsymbol{q}$ is the charge of a single charge carrier
- $\boldsymbol{F}$ is the force
- $\boldsymbol{E}$ is the applied electric field to the charge carrier

If the ***Equ.* 3.14** is applied, the electrostatic force is given by the ***Equ.* 3.15** and ***Equ.* 3.16**: [1] [16]

$$f^{+}_{E_{dc}}(x) = \frac{1}{2}\sigma^{+}E_{dc}(x) = \frac{1}{2}\varepsilon {E_{dc}}^{2}(x) \tag{3.15}$$

$$f^{-}_{E_{dc}}(x) = \frac{1}{2}\sigma^{-}E_{dc}(x) = \frac{1}{2}\varepsilon E^2_{dc}(x) \tag{3.16}$$

$$\Delta f^{\rho}_{E_{dc}}(x) = \rho(x)\Delta x E_{dc}(x) \tag{3.17}$$

- $\boldsymbol{f^{+}_{E_{dc}}(x), f^{-}_{E_{dc}}(x)}$ forces acting on surface charges: $\boldsymbol{\sigma^{+}(x), \sigma^{-}(x)}$
- $\boldsymbol{\Delta f^{\rho}(x)}$ force acting on thin space charge layer: $\boldsymbol{\Delta x}$

The force originating from the DC voltage source due to the Laplace field can be neglected. The field generates a constant force and thus also a constant pressure wave. Therefore, in this case only the ***Equ.* 3.18 – 3.20**, which are responsible for the charge vibration are taken into account. [16] [18]

$$f_{e_p}^{+}(t) = \sigma^{+} e_p(t) + \frac{1}{2}\varepsilon e_p^2(t) = [\sigma^{+} + \frac{1}{2}\varepsilon e_p(t)]e_p(t) \tag{3.18}$$

$$f_{e_p}^{-}(t) = \sigma^{-} e_p(t) - \frac{1}{2}\varepsilon e_p^2(t) = [\sigma^{-} + \frac{1}{2}\varepsilon e_p(t)]e_p(t) \tag{3.19}$$

$$\Delta f_{e_p}^{\rho}(x,t) = \rho(x)\Delta x e_p(t) \tag{3.20}$$

3.3 Generation and Propagation of Acoustic Waves

The vibration of the charges, due to the force $\boldsymbol{f_{e_p}(t)}$ generates acoustic waves that propagate through the PEA cell. When the acoustic wave reaches an interface of two different materials with different acoustic impedances, one part of the wave is reflected and another is transmitted. These phenomena are described by the coefficients: generation $\boldsymbol{K_{i-j}^{G}}$, transmission $\boldsymbol{K_{i-j}^{T}}$ and reflection $\boldsymbol{K_{i-j}^{R}}$ in the following equations. [16]

$$K_{i-j}^{G} = \frac{Z_j}{Z_i + Z_j} \tag{3.21}$$

$$K_{i-j}^{T} = \frac{2Z_j}{Z_i + Z_j} \tag{3.22}$$

$$K_{i-j}^{R} = \frac{Z_j - Z_i}{Z_i + Z_j} \tag{3.23}$$

As already mentioned, these coefficients depend on the acoustic impedance $\boldsymbol{Z}$, which in turn is a product of the mass density and the acoustic velocity of the medium. The lowered letters indicate the material from which the acoustic wave is generated or coming from ($\boldsymbol{i}$) and the material to which it propagates, $\boldsymbol{j}$. [16]
Using the propagation velocity $\boldsymbol{v}$ of the material $\boldsymbol{i}$ and the strength of the material $\boldsymbol{d_x}$ that the acoustic wave must pass, the propagation time $\boldsymbol{\tau_x}$ of the wave can be calculated using the following equation: [16]

$$\tau_x = \frac{d_x}{v_i} \tag{3.24}$$

To illustrate this ***Fig.* 3** shows the generation and transmission coefficient at the interfaces of the materials and in the bulk.

The subscripts AL stands for Aluminium, A for specimen A and PVDF is the Piezo electric sensor.

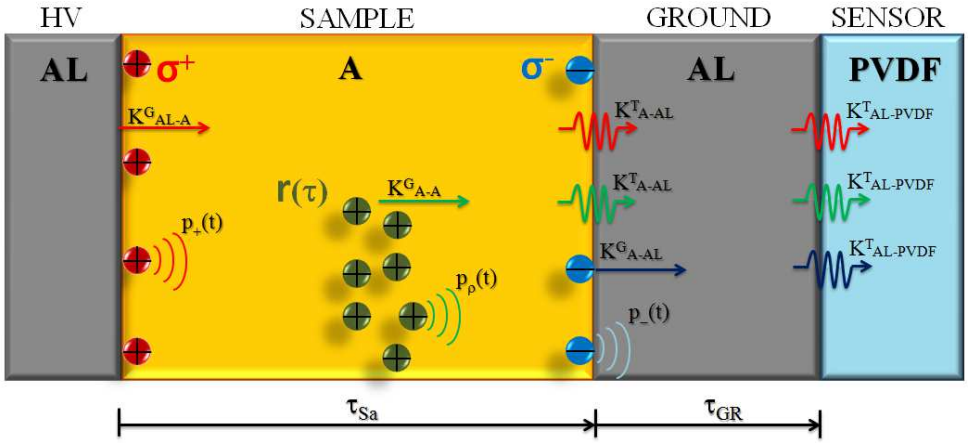

Figure 3: generation and propagation of acoustic waves source: [16]

If ***Fig.* 3** is used for illustration, then an acoustic wave is generated ($\boldsymbol{K^G_{Al-A}}$), due to the surface charge on the high voltage electrode. The generation of it can be calculated with ***Equ.* 3.25**. This wave then propagates through the test specimen ***A*** until it meets the ground electrode, due to the different impedances of the media ($\boldsymbol{K^T_{A-AL}}$) is calculated with ***Equ.* 3.26**. Once the wave has finally propagated through the ground electrode to the piezoelectric sensor, the last interface between the ground electrode and the piezoelectric sensor has to be mastered($\boldsymbol{K^T_{AL-PVDF}}$). This interface is calculated with ***Equ.* 3.27**. [16]

$$K^G_{AL-A} = \frac{Z_A}{Z_{AL} + Z_A} \tag{3.25}$$

$$K^T_{A-AL} = \frac{2Z_{AL}}{Z_A + Z_{AL}} \tag{3.26}$$

$$K^T_{AL-PVDF} = \frac{2Z_{PVDF}}{Z_{AL} + Z_{PVDF}} \tag{3.27}$$

The acoustic wave generated by the negative charges at the ground electrode can be seen in ***Equ.* 3.28**. The coefficient $\boldsymbol{K^T_{AL-PVDF}}$ is the same as in ***Equ.* 3.27**. [16]

$$K^G_{A-AL} = \frac{Z_{AL}}{Z_A + Z_{AL}} \tag{3.28}$$

If the acoustic wave is generated by space charge in the bulk. The generation coefficient for homogeneous materials is calculated as follows:

$$K^G_{A-A} = \frac{Z_A}{Z_A + Z_A} = 0.5 \tag{3.29}$$

The value of **0.5** means that the wave propagates with **50%** in both directions. The transmission coefficients for the next material interfaces are calculated as already presented in ***Equ.* 3.26** and ***Equ.* 3.27**. The calculated propagation time for ***Fig.* 2** results in two different propagation times. Where $\boldsymbol{\tau_A}$ is the propagation time of the sample and $\boldsymbol{\tau_{GR}}$ is the propagation time of the ground electrode. [16]

$$\tau_A = \frac{d_A}{v_A} \tag{3.30}$$

$$\tau_{GR} = \frac{d_{GR}}{v_{AL}} \tag{3.31}$$

- $\boldsymbol{d_A, d_{GR}}$ thickness of the specimen and the ground electrode
- $\boldsymbol{v_A, v_{AL}}$ speed of sound in the specimen and the ground electrode

The calculated acoustic pressure wave $\boldsymbol{p(t)}$ propagating towards the piezo electric sensor($\boldsymbol{PVDF}$), based on the surface charges $\boldsymbol{\sigma^+, \sigma^-}$ and the space charge $\boldsymbol{\rho(x)}$ are calculated as follows: [16]

$$p_+(t) = K^G_{AL-A} K^T_{A-AL} K^T_{AL-PVDF}\ f^+_{e_p}(t) \tag{3.32}$$

$$p_-(t) = K^G_{A-AL} K^T_{AL-PVDF}\ f^-_{e_p}(t) \tag{3.33}$$

$$\Delta p_\rho(x,t) = K^G_{A-A} K^T_{A-AL} K^T_{AL-PVDF}\ \Delta f^\rho_{e_p}(x,t) \tag{3.34}$$

If the propagation times for the acoustic waves $\boldsymbol{\tau_A}$ and $\boldsymbol{\tau_{GR}}$ of the test specimen and the ground electrode are now substituted into the ***Equ.* 3.32 – 3.34**, they can be rewritten as follows: [16]

$$p_+(t) = K^G_{AL-A} K^T_{A-AL} K^T_{AL-PVDF}\ [\sigma^+ + \frac{1}{2}\varepsilon e_p(t-\tau_A-\tau_{GR})] e_p(t-\tau_A-\tau_{GR}) \tag{3.35}$$

$$p_-(t) = K^G_{A-AL} K^T_{AL-PVDF}\ [\sigma^- - \frac{1}{2}\varepsilon e_p(t-\tau_{GR})] e_p(t-\tau_{GR}) \tag{3.36}$$

$$\Delta p_\rho(x,t) = K^G_{A-A} K^T_{A-AL} K^T_{AL-PVDF}\ \rho(x)\Delta x e_p(t - \frac{d_A - x_\rho}{v_A} - \tau_{GR}) \tag{3.37}$$

The acoustic wave generated by a thin layer of space charge $\boldsymbol{\Delta x}$ is indicated by the term $\boldsymbol{x_\rho}$ at a generic position in the specimen. The space charge position is described starting from the high voltage electrode at the location $\boldsymbol{d_A - x_\rho}$. All acoustic waves caused by the accumulated space charge are described by ***Equ.* 3.38**. Here, $\boldsymbol{d_A - x_\rho}$ from ***Equ.* 3.37** is substituted by the product of the propagation velocity $\boldsymbol{v_A}$ with the propagation time $\boldsymbol{\tau}$.

The propagation velocity substituted into the equation is constant and the propagation time $\boldsymbol{\tau}$ is defined from a generic position in the specimen. [16]

$$p_\rho(t) = 0.5 K^T_{A-AL} K^T_{AL-PVDF}\ v_A \int_0^t r(\tau) e_p(t - \tau - \tau_{GR}) d\tau \tag{3.38}$$

As already shown, the value of **0.5** is calculated in homogeneous materials as the generation coefficient(***Equ.* 3.29**). Finally, all generated acoustic waves $\boldsymbol{p_{tot}(t)}$ are added together. ***Equ.* 3.39** now describes the acoustic wave generated by an electric pulse without reflection coefficient. The surface charges can be considered as start and end point of the region of interest. [16] [18] [20]

$$\begin{aligned}
&p_{tot}(t) = p_+(t) + p_-(t) + p_\rho(t) = \\
&K^G_{AL-A} K^T_{A-AL} K^T_{AL-PVDF}\ [\sigma^+ + \frac{1}{2}\varepsilon e_p(t - \tau_A - \tau_{GR})] e_p(t - \tau_A - \tau_{GR}) + \\
&K^G_{A-AL} K^T_{AL-PVDF}\ [\sigma^- - \frac{1}{2}\varepsilon e_p(t - \tau_{GR})] e_p(t - \tau_{GR}) + \\
&0.5 K^T_{A-AL} K^T_{AL-PVDF}\ v_A \int_0^t r(\tau) e_p(t - \tau - \tau_{GR}) d\tau
\end{aligned} \tag{3.39}$$

3.4 Acoustic Wave Reflections

The resulting reflections of acoustic waves, at interfaces of different acoustic impedances, have not yet been taken into account and may lead to an incorrect interpretation of the measurement result. How to calculate the reflection coefficient to be considered has already been shown with ***Equ.* 3.23**. At the same impedance, when $\boldsymbol{Z_i = Z_j}$, the coefficient becomes 1 and the travelling wave is not affected by the interface of the Materials. Assuming this scenario, the signal recorded by the piezo electric sensor must have only two peaks in the signal, that is of the surface charges. To prevent these reflections, ***Inequ.* 3.40** and ***Inequ.* 3.41** must be satisfied for the ground electrode and the absorber. [16] [21]

$$d_{GR} > \frac{1}{2} d_A \frac{v_{AL}}{v_A} \tag{3.40}$$

$$d_{ABS} > \frac{1}{2} d_A \frac{v_{PVDF}}{v_A} \tag{3.41}$$

- $\boldsymbol{d_A}$ thickness of specimen
- $\boldsymbol{v_{AL}, v_A, v_{PVDF}}$ speed of sound for the specimen and for aluminium as well as for the absorber material

3.5 Output Signal of the Piezoelectric Sensor

If the acoustic wave $\boldsymbol{p_{tot}(t)}$ reaches the piezoelectric sensor, then a charge is induced on the surface due to the piezoelectric effect. The amount of charge depends on the pressure wave $\boldsymbol{p}$, the piezo electric constant $\boldsymbol{P_c}$ and the area $\boldsymbol{S}$ of the sensor. [16]

$$q(t) = P_c S p_{tot}(t) \tag{3.42}$$

The recorded signal, the voltage $\boldsymbol{V_{PVDF}(t)}$, is calculated with the static capacitance $\boldsymbol{C_p}$ of the sensor, which is equal to that of a plate capacitor: [16]

$$V_{PVDF}(t) = \frac{q(t)}{C_p} \tag{3.43}$$

$$C_p = \frac{\varepsilon S}{d_{SE}} \tag{3.44}$$

where $\boldsymbol{\varepsilon = \varepsilon_0 \varepsilon_{PVDF}}$ and $\boldsymbol{d_{SE}}$ is the thickness of the piezo electric sensor. By substituting ***Equ.* 3.44** into ***Equ.* 3.43** the resulting ***Equ.* 3.45** is shown below: [16]

$$V_{PVDF}(t) = \frac{q(t)}{C_p} = \frac{P_c\ S\ p_{tot}}{\varepsilon \frac{S}{d_{SE}}} = \frac{P_c\ d_{SE}}{\varepsilon} p_{tot}(t) \tag{3.45}$$

According to the resulting ***Equ.* 3.45**, the recorded voltage $\boldsymbol{V_{PVDF}(t)}$ depends on the pressure $\boldsymbol{p_{tot}(t)}$ and the thickness $\boldsymbol{d_{SE}}$ of the sensor. [16]

3.6 Deconvolution Process

The coupling between amplifier and transducer is that of a high-pass filter according to the scheme of an $\boldsymbol{RC-element}$. Due to this, the recorded electrical signal is distorted and must be corrected later with the help of a deconvolution process. Assuming the same Device Under Test (=DUT) as in ***Fig.* 2**, the perfect response of the recorded acoustic pulse looks like in ***Fig.* 4**, but due to the distortion the real recorded pulse seems like somewhat similar to ***Fig.* 5**. The red circle in ***Fig.* 5** indicates the distorted region of the signal. If this phenomenon can be observed right after starting the measurement, it's a distortion of the $\boldsymbol{RC-element}$, since it can't be charge as charge needs time to accumulate in the bulk. However, if the measurement has been in progress for a while, it is very difficult to differentiate whether it is accumulated charge or a distorted measurement. Furthermore, it must be mentioned that the measurement error as shown in the red circles, as can be seen in ***Fig.* 5** differs very much from dielectric to dielectric material under test. [16]

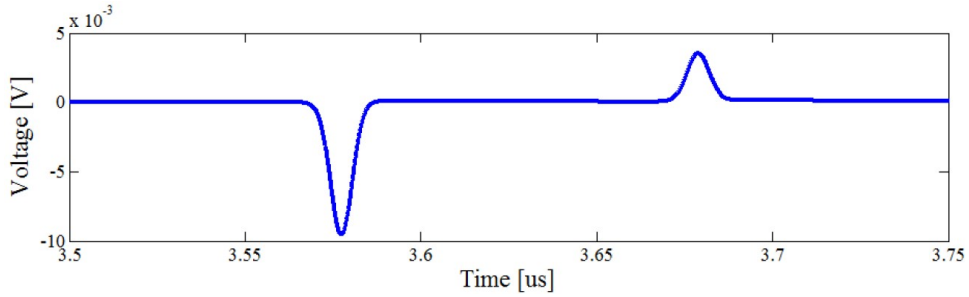

Figure 4: ideal charge response of the acoustic pressure wave source: [16]

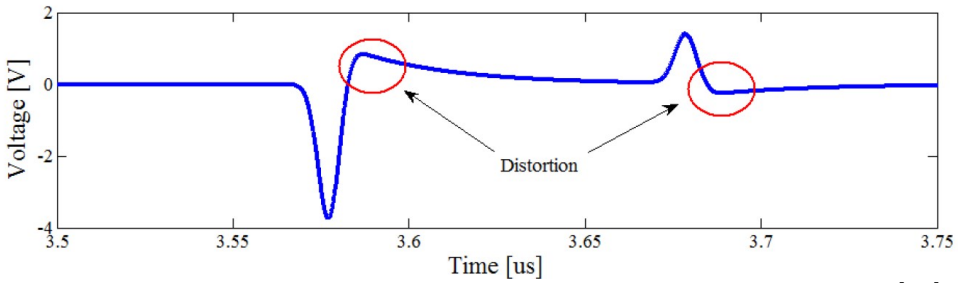

Figure 5: real charge response of the acoustic pressure wave source: [16]

The most commonly used method for the deconvolution process was developed by Jeroensen [22]. This method allows the deconvolution process to start with the recorded signal from the oscilloscope, as can be seen in ***Equ.* 3.46**: [16]

$$V_{det}(t) = F^{-}1[V_{orig}(f) * H(f)] \tag{3.46}$$

By rewritting ***Equ.* 3.46** for the original deconvoluted Signal, the equation changes to: [16]

$$V_{dec}^{orig}(t) = F^{-1}[\frac{V_{det}(f)}{H(f)}] \tag{3.47}$$

- $\boldsymbol{F^{-1}}$ inverse fourier transform
- $\boldsymbol{H(f)}$ system response
- $\boldsymbol{V_{det}}$ detected signal at the oscilloscope

If $\boldsymbol{H}$ is known, it is possible to reconstitute the original signal with the inverse of $\boldsymbol{H^{-1}}$. [16] The connection between the signals $\boldsymbol{V_{det}(t)}, \boldsymbol{\rho(t)}$ the pressure $\boldsymbol{p(t)}$, the pulse voltage $\boldsymbol{e_p(t)}$ and the detection system response in time domain $\boldsymbol{h(t)}$ are as follows: [16]

$$V_{det}(t) = Kh(t) \otimes e_p(t) \otimes \rho(t) \tag{3.48}$$

- $\boldsymbol{K}$ calibration factor
- $\otimes$ represents convolution operation

The system response $\boldsymbol{H(t)}$ results from the convoluted signal from $\boldsymbol{h(t)}$ with $\boldsymbol{e_p(t)}$. For this reason, the previously noted ***Equ.* 3.48** can be rewritten in the frequency domain to: [16]

$$V_{det}(f) = Kh(f)e_p(f)\rho(f) = kH(f)\rho(f) \tag{3.49}$$

The already mentioned space charge distribution $\boldsymbol{\rho(t)}$ can be evaluated in the time domain as well as in the frequeny domain, with the folowing ***Equ.* 3.50** and ***Equ.* 3.51** [16]

$$\rho(f) = \frac{1}{K}\frac{V_{det(t)}}{H(f)} \tag{3.50}$$

$$\rho(t) = \frac{1}{K}F^{-1}[\frac{V_{det}(t)}{H(f)}] \tag{3.51}$$

As soon as a known space charge $\boldsymbol{\rho(t)}$ is measured with the help of the piezo electric sensor $\boldsymbol{V_{det}(t)}$, the response function $\boldsymbol{H}$ can be calculated. It should be noted, however, that only the charge on the surfaces $\boldsymbol{\sigma}$ interfaces of the electrodes can be predicted with ***Equ.* 3.5** and ***Equ.* 3.6**. However, since the voltage pulse, from the positive surface charge, must pass through the entire specimen, the pulse is subject to very high attenuation and dispersion. Therefore, due to the same magnitude in charge $\boldsymbol{\sigma^- = \sigma^+}$, the negative surface charge $\boldsymbol{\sigma^-}$ is mainly used as this pulse $\boldsymbol{V_{gr}}$ is not subjected to any damping or dispersion. [16]

$$H(f) = \frac{V_{det}(f)}{K\rho(f)} = \frac{V_g r}{K\sigma^-} \tag{3.52}$$

With the impulse funtion $\boldsymbol{\delta(t)}$ by assuming the following:

$$K_1 = K\sigma^- \tag{3.53}$$

***Equ.* 3.52** can be rewritten and changes to:

$$H(f) = \frac{V_{gr}(f)}{K\sigma^-} = \frac{1}{K_1}V_{gr} \tag{3.54}$$

$\boldsymbol{K_1}$ represents the ideal signal from the surface charge $\boldsymbol{\sigma^-}$ without distortion of the RC-element. However, in ***Equ.* 3.47** the inverse of the system response $\boldsymbol{H(f)}$ is needed. Therefore, the inverse of ***Equ.* 3.54** leads to: [16]

$$H(f)^{-1} = \frac{K_1}{V_{gr}(f)} \tag{3.55}$$

Another problem which arise during the deconvolution process are the high frequency components, in the signal $\boldsymbol{H(f)^{-1}}$. To avoid the distortion by the high frequency com-

ponents in the signal a low pass Gaussian filter $\boldsymbol{G(f)}$ is applied to the signal with the task to remove these components. [16] According to ***Equ.* 3.47**, the inverse system response $\boldsymbol{H(f)^{-1}}$ is still multiplied by the recorded signal $\boldsymbol{V_{det}(f)}$. After that the inverse Fourier transform$\boldsymbol{F^{-1}}$ has to be done to get the original charge profile. Now a correction factor must be included $\boldsymbol{K_{corr}}$, because $\boldsymbol{V_{dec}}$ is an approximation of the real charge profile $\boldsymbol{K_1}$ was assumed as 1. [16]

$$K_{corr} = \frac{max(|V_{dec}(t)|)}{max(|V_{det}(t)|)} \tag{3.56}$$

To get the real charge profile with the Correction factor according to the applied voltage, $\boldsymbol{V_{dec}(t)}$ has to be divided by the Correction factor $\boldsymbol{K_{corr}}$:

$$V_{dec}^{orig}(t) = \frac{V_{dec}(t)}{K_{corr}} \tag{3.57}$$

The above mathematical description of the deconvolution process is also shown as a block diagram in ***Fig.* 6**. [16]

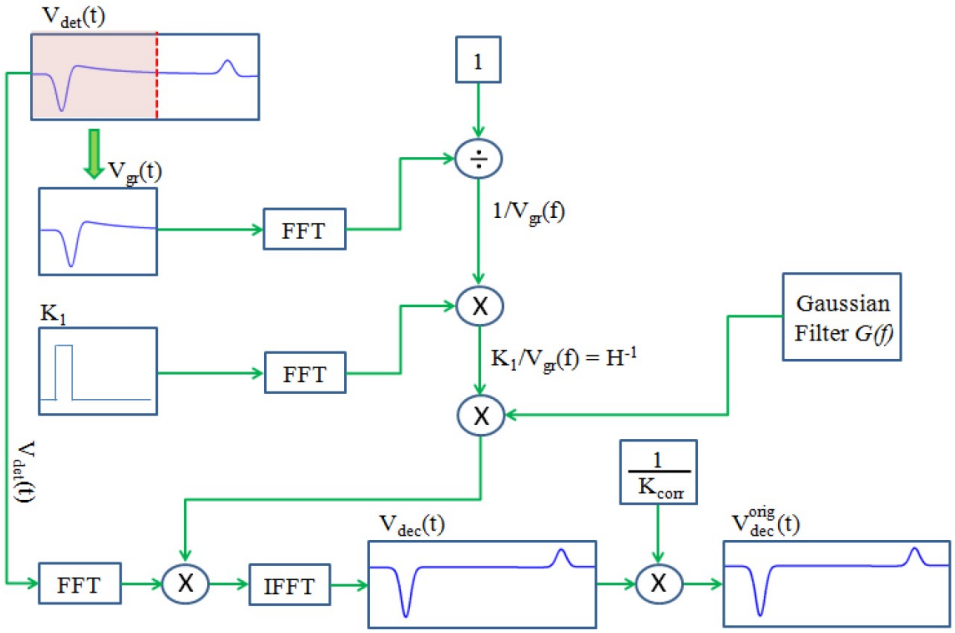

Figure 6: Block diagram of the deconvolution process source: [16]

3.7 Calibration Process

The signal $\boldsymbol{V_{dec}^{orig}}$ now obtained is proportional to the applied voltage, but this is still in units of $[\boldsymbol{mV}]$ but the space charge profile $\boldsymbol{\rho(x)}$ should be in $[\boldsymbol{C/m^3}]$. Therefore, two calibrations are necessary. First, the X-axis must be calibrated from a time-resolved to a displacement-resolved axis, and second, the voltage signal must be adjusted to match the charge signal, as shown in ***Fig.* 7**. [16]

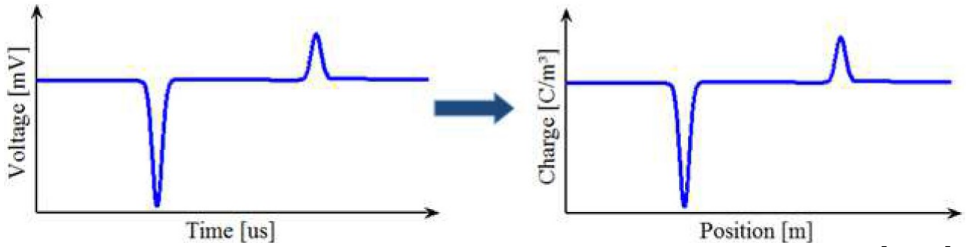

Figure 7: Necessary Calibration from the recorded PEA signal in $[\boldsymbol{mV}]$ to the charge profile in $[\boldsymbol{C/m^3}]$ source: [16]

To convert the time-resolved axis to a displacement-resolved axis, the speed of sound of the material under test must be known, since the times for the two largest amplitude values of the incoming waves are known from the measurement itself. Based on this information, the two peak values can be determined as follows: [16]

$$position = v_i time \tag{3.58}$$

If the calibration procedure has been done correct, the displacement between the peaks should be of the same thickness $\boldsymbol{d_a}$ as the specimen itself. In order to start the displacement value from 0 with the help of the calibration, the ***delay time*** of the incoming negative wave must be adjusted, since it depends on the thickness $\boldsymbol{d_a}$ and on the speed of sound of the ground electrode $\boldsymbol{v_{al}}$. ***Fig.* 8** serves as an illustration and shows the delay caused by the ground electrode. [16]

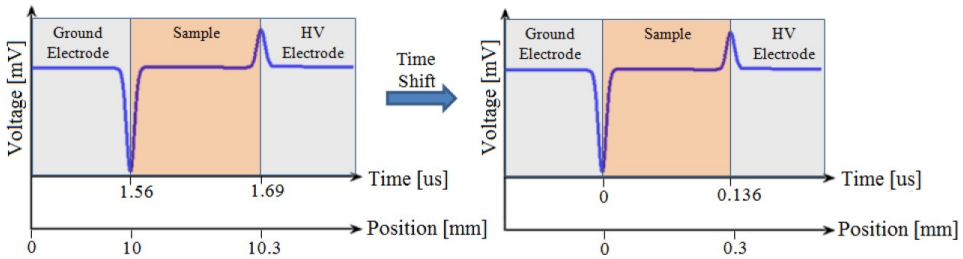

Figure 8: delay correction of the ground electrode source: [16]

Now, as already mentioned, a calibration of the y-axis is necessary to change the voltage signal into a space charge density. For this purpose, another calibration factor $\boldsymbol{K_{cal}}$ is introduced. After the calibration to the displacement axis has been performed, the

obtained signal can now be written after the deconvolution process as follows $\boldsymbol{V_{dec}^{orig}(x)}$. The connection between the signal and the calibration factor $\boldsymbol{K_{cal}}$ is now as follows: [16]

$$K_{cal} = \frac{V_{dec}^{orig}(x)}{\rho(x)} \tag{3.59}$$

The determination of the calibration factor can only be done with the surface charge($\boldsymbol{\sigma}$), since this charge density is known. As already explained in the ***chapter* 3.6**, the same problems with the wave beginning from the positive electrode occur here. Therefore, only the negative wave is used for this purpose.
Assuming that the applied voltage $\boldsymbol{V}$ is known, the electric field $\boldsymbol{E}$ is calculated with the material thickness $\boldsymbol{d_a}$ for a homogeneous electrode arrangement. [16]

$$E = \frac{V}{d_a} \tag{3.60}$$

This ***Equ.* 3.60** is only valid if no polarization or charge injection process has taken place. If this was not the case, the surface charge can be calculated like in ***Equ.* 3.6**. With this provided information ***Equ.* 3.59** changes to: [16]

$$K_{cal} = \frac{\int_{x_a}^{x_b} V_{dec}^{orig}(x)dx}{\sigma^-} \tag{3.61}$$

The start and end points of the Integral in ***Equ.* 3.61** are related to the start and end point of the $\boldsymbol{V_{dec}^{orig}}$ signal. The integral of it represents the area of the negative voltage curve, which is related to the negative charge density. After the calibration factor is known the space charge density can be calculated: [16]

$$\rho(x) = \frac{V_{dec}^{orig}(x)}{K_{cal}} \tag{3.62}$$

4 Measurement Setup

This section shows the measurement setup for the Pulsed electro-acoustic method to perform Space charge measurements, as can be seen in ***Fig.* 9** under DC. In between the layers beginning with the HV to the Ground electrode, an oil droplet has been placed to reduce the acoustic impedance. The Pulse duration send by the Pulse Generator is **5** $\boldsymbol{ns}$ and the frequency of the Pulse is $\mathbf{3,7}\ \boldsymbol{kHz}$. The specimen for the PEA-method has a thickness of $\mathbf{0.127}\ \boldsymbol{mm}$. The temperature during the measurement was below $\mathbf{25°}\boldsymbol{C}$.To simulate the structure of a cable, a semiconductor material was given in addition to the material.

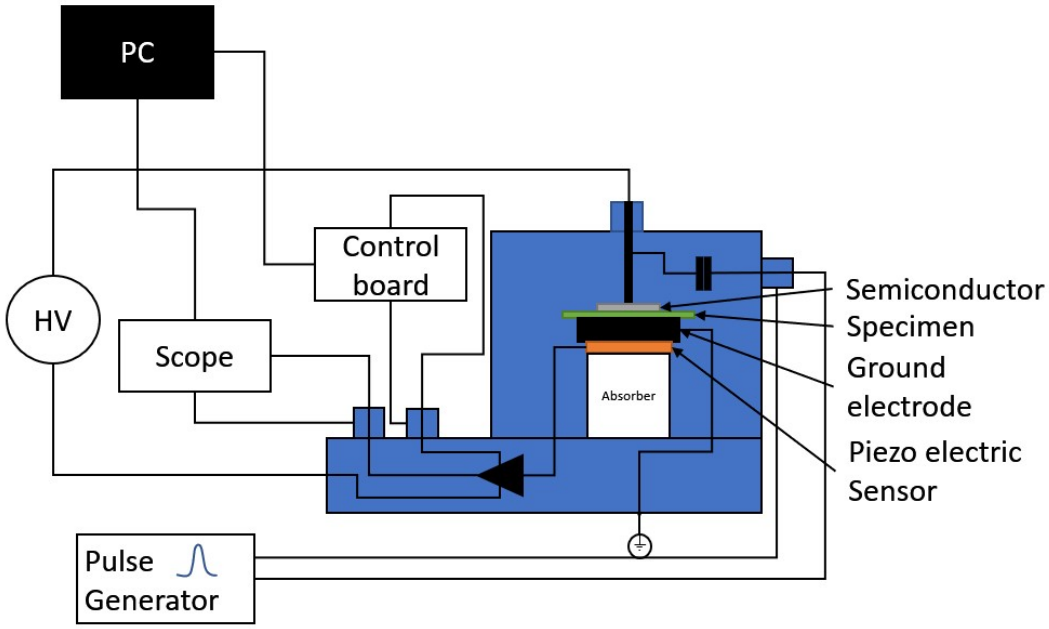

Figure 9: Measurement Setup of the Pulsed electro-acoustic method

4.1 Measurement Procedure

1. Loading the PEA-cell
2. Set up the circuit according to ***Fig.* 9**
3. Check the connection between the PC and the Scope and see whether it is possible to read data from the scope
4. Insert the Material specifications and important parameters in the PEALabV4 interface of the MATLAB application
5. Increase the voltage to the desired level
6. press the start button

7. Wait until the poling time has ended
8. Press the depolarization button immediately after the end of the poling time.
9. The measurement ends automatically after the depoling time has ended
10. Save the results

5 Measurement Results

This section shows the results of the Space Charge Measurement with the Pulsed Electro Acoustic method.

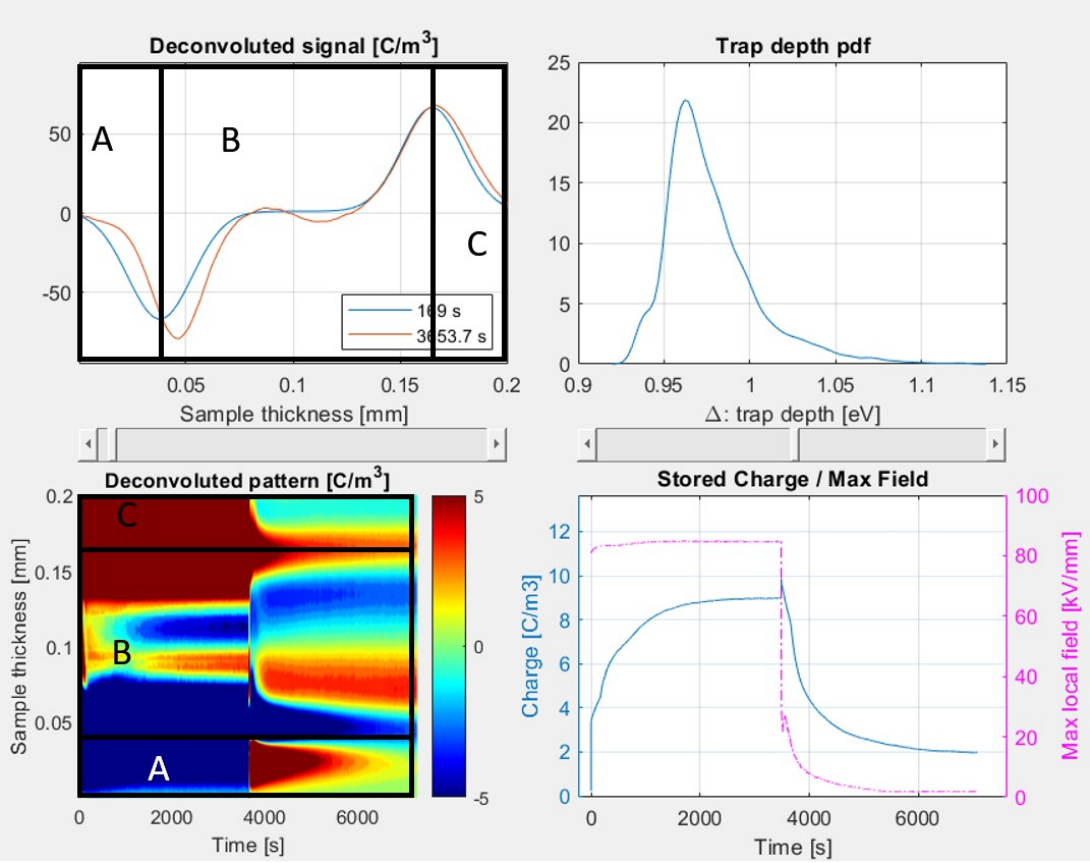

Figure 10: Kapton 80kV/mm at a thickness of 0.127mm >1h poling time

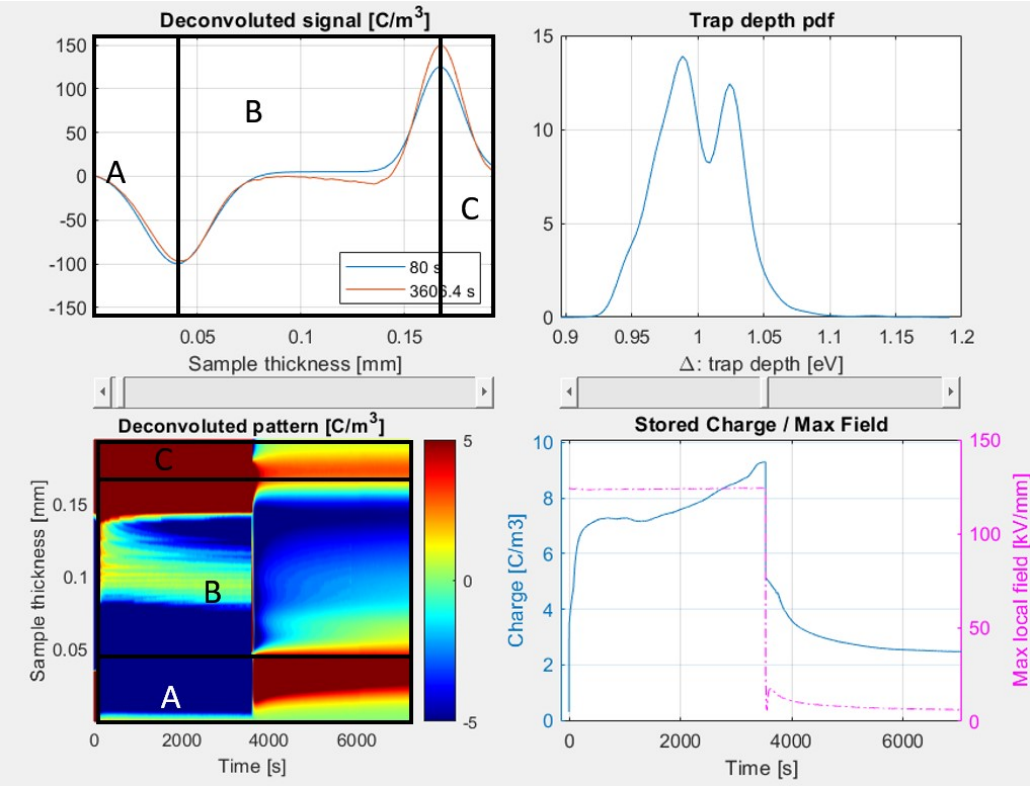

Figure 11: Kapton 120kV/mm at a thickness of 0.127mm >1h poling time

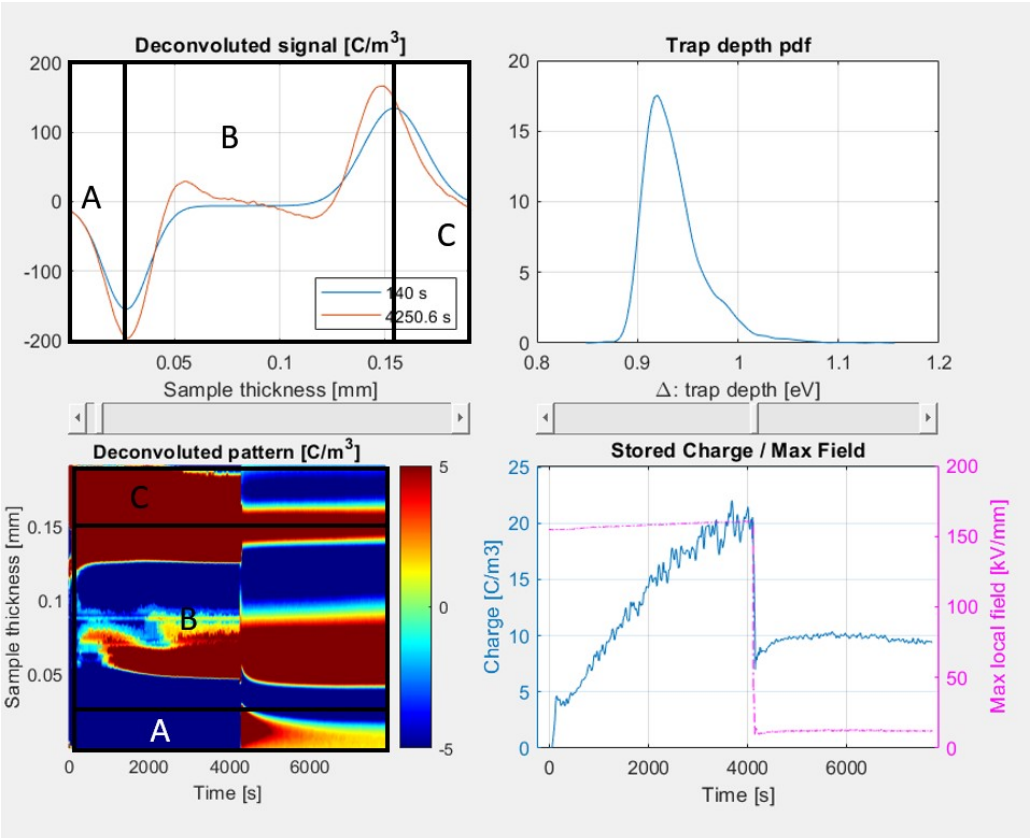

Figure 12: Kapton 150kV/mm at a thickness of 0.127mm >1h poling time

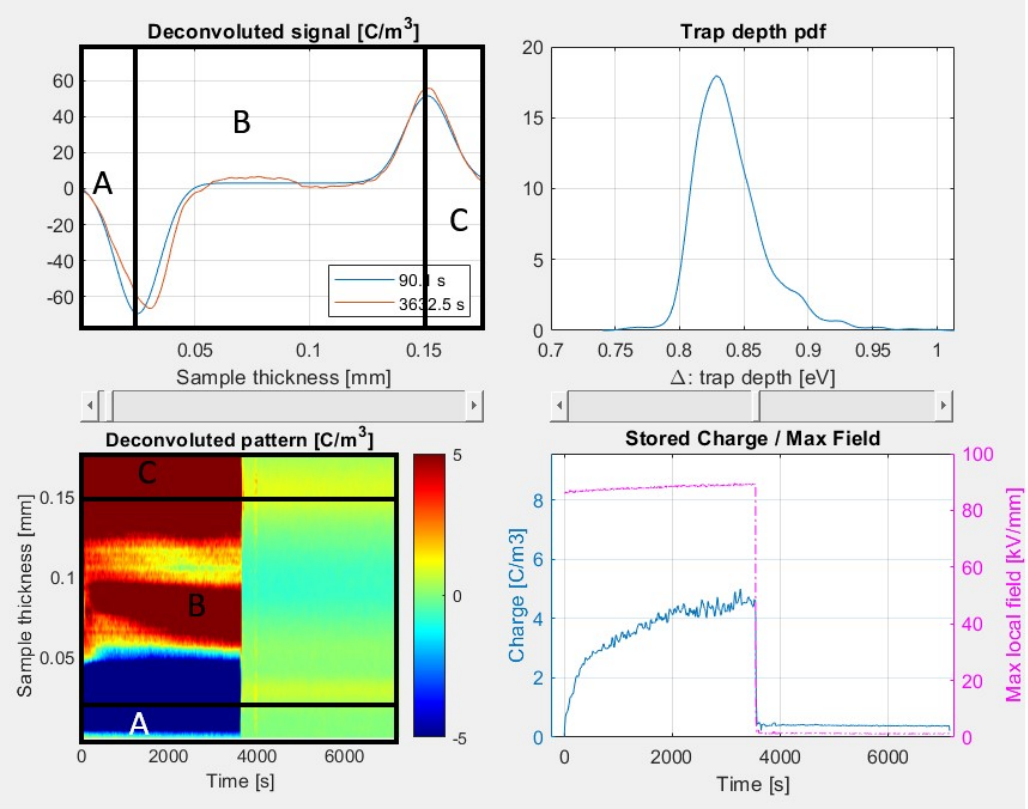

Figure 13: Fluorinated Ethylene Propylene 80kV/mm at a thickness of 0.127mm >1h poling time

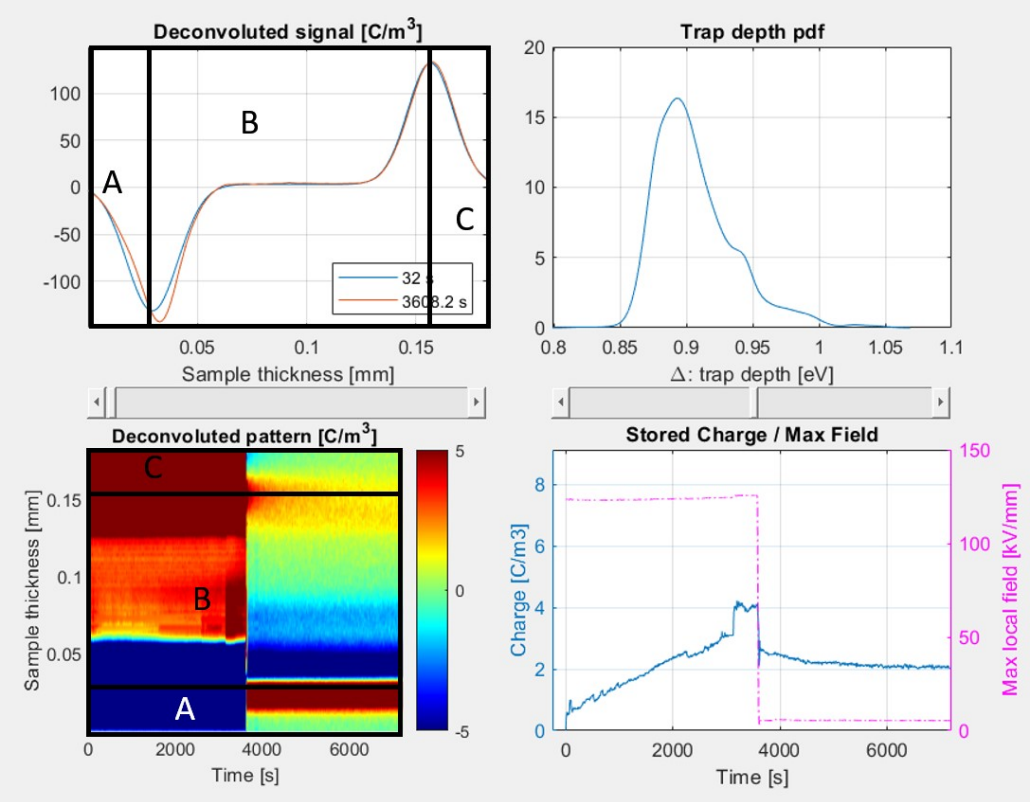

Figure 14: Fluorinated Ethylene Propylene 120kV/mm at a thickness of 0.127mm >1h poling time

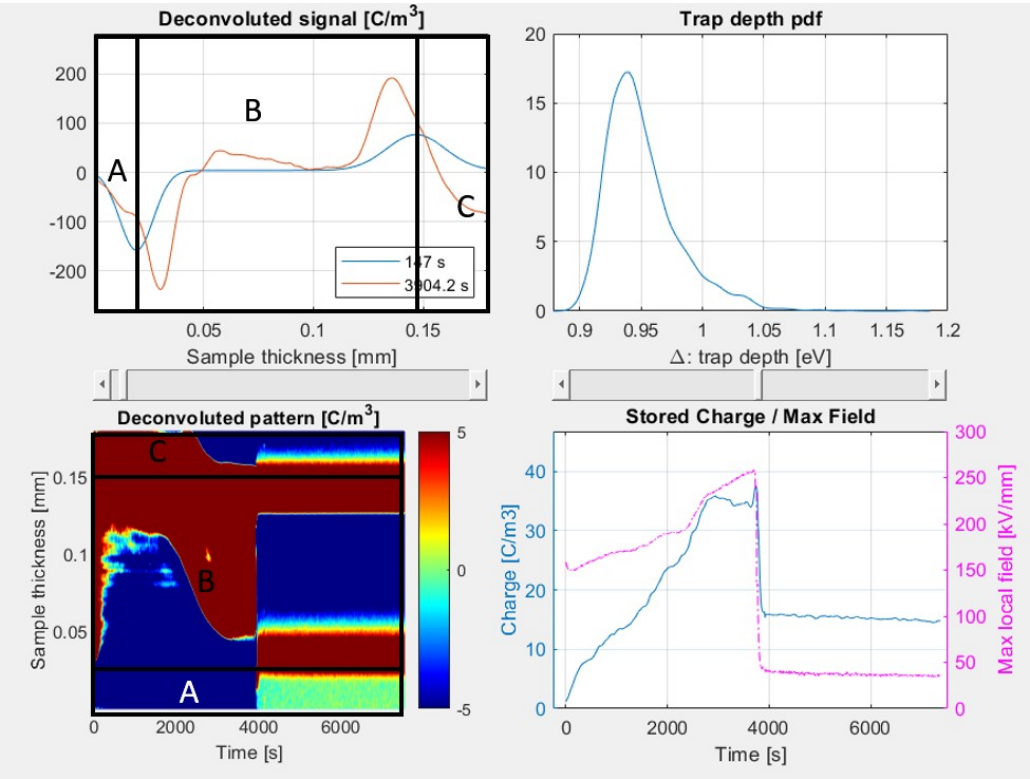

Figure 15: Fluorinated Ethylene Propylene 150kV/mm at a thickness of 0.127mm >1h poling time

6 Discussion

Measurements were made with both DUTs at $\mathbf{80kV/mm}$, $\mathbf{120kV/mm}$ and $\mathbf{150kV/mm}$. The results are sorted by test specimen and by increasing electric field. It can be seen that the increase in field strength leads to an increase in the injection of charge carriers, or/and the effect of polarization. This is the case for both materials and can be seen in the figure with the heading ***stored charge***. Likewise, the energy level of the charge carriers in deep traps increases with increasing field strength, as can be seen from the figure ***trap depth***.

The ***deconvoluted Signal*** from voltage to charge carrier density shows how the signal changes at the beginning of the measurement until the end of polarization. The contour plot of the charge carrier density shows how this changes as a function of the measurement time and the thickness of the test specimen.

The recorded accumulated charge density is divided in **3 *Sections***. Firstly, the two surface charges which accumulate at the Cathode (ground electrode ***A***) and at the Anode (high voltage electrode **(*C*)**). As well as in the test specimen **(*B*)**, in which it can be observed how the charge distribution is aligned on the basis of the applied voltage and also how charge is induced. It is worth noting that the measurements in ***Fig.* 15** show how charge injection and transportation in terms of holes takes place from the Anode to the Cathode when the principle of the energy band model of charge transportation is applied, as it can be used in Semiconductors. [20] Especially with Kapton, the accumulation of hetero charge at the interfaces to the electrodes can be observed.Whereas with FEP the accumulation of homo charge is noticeable.

The peak in the ***stored charge*** figure right after the voltage turn off happens because of the way the scope records the measurement. Since the environment of the lab, where the measurement have been taken, has a really high noise level and no Faraday cage, a high averaging filter was applied to the recorded signal to smooth the data. In addition to this after the program has been started it automatically adjusts the voltage per division for its best resolution without clipping. After the voltage is switched off a change in the recording voltage is observable and the scope adjusts the voltage per division again and therefore also the trigger is forced again and the averaging of the signal starts from 0 again. This leads to high noise level in the measured data and results in this peak. This can be seen in ***Fig.* 10** and ***Fig.* 15**

7 Conclusion

The whole measuring system and their results must be considered very critically. In principle, it depends on the magnitude of the normal field component of the electric field whether charge is induced into the material or not. However, due to the electrode arrangement and the triple point [4], field excesses occur at this point which far exceed the calculated uniform field distribution. Therefore, the electric field strength with which the material was stressed is actually three times the magnitude or even higher. [4]

Nevertheless, the space charge measurement technique offers a new way to check electrical insulations. The materials tested in this report (Kapton,FEP) store beyond the applied 120kV/mm a significant amount of space charge over a longer period of time. This injected charge can itself be damaging to the insulation, but it can also trigger premature partial discharge in a cavity, depending on the type of charge accumulation. It should also be mentioned that the injection of charge carriers is strongly dependent on temperature, since the conductivity also changes strongly with this. [23]

List of Figures

References

[1] Wolfgang Mathis and Albrecht Reibiger. *Küpfmüller Theoretische Elektrotechnik: Elektromagnetische Felder, Schaltungen und elektronische Bauelemente*. Springer Berlin Heidelberg, Berlin, Heidelberg, 20. aufl. 2017 edition, 2017.

[2] Dierk Schröder, editor. *Leistungselektronische Schaltungen: Funktion, Auslegung und Anwendung*. Springer Vieweg, Berlin, Germany, 2019]-.

[3] René Flosdorff and Günther Hilgarth. *Elektrische Energieverteilung: Mit 47 Tafeln und 71 Beispielen*. Leitfaden der Elektrotechnik. Teubner, Stuttgart, 6., überarb. aufl. edition, 1994.

[4] Andreas Küchler. *High Voltage Engineering: Fundamentals - Technology - Applications*. Springer eBook Collection Engineering. Springer Vieweg, Berlin, Heidelberg, 5th ed. 2018 edition, 2018.

[5] Artur Robert v. Hippel. *Dielectrics and waves: Arthur [Artur] R[obert] v. Hippel*. Wiley usw, New York, (1954).

[6] Frederik H. Kreuger and F. H. Kreuger. *Industrial high DC voltage: 1. fields, 2. breakdowns, 3. tests*. Delft Univ. Press, Delft, 1995.

[7] Wolfgang Hauschild and Eberhard Lemke. *High-voltage test and measuring techniques*. Springer, Berlin and Heidelberg and New York and Dordrecht and London, 2014.

[8] C. Laurent, G. Teyssedre, S. Le Roy, and F. Baudoin. Charge dynamics and its energetic features in polymeric materials. *IEEE Transactions on Dielectrics and Electrical Insulation*, 20(2):357–381, 2013.

[9] M. Taleb, G. Teyssedre, S. Le Roy, and C. Laurent. Modeling of charge injection and extraction in a metal/polymer interface through an exponential distribution of surface states. *IEEE Transactions on Dielectrics and Electrical Insulation*, 20(1):311–320, 2013.

[10] Frank Messerer. *Gas-insullated substation (GIS) for HVDC: Zugl.: München, Techn. Univ., Diss., 2001*, volume 319 of *Fortschritt-Berichte VDI Reihe 21, Elektrotechnik*. VDI-Verl., Düsseldorf, als ms. gedr edition, 2002.

[11] Manfred Beyer. *Hochspannungstechnik: Theoretische und praktische Grundlagen [für die Anwendung]*. Springer, Berlin etc., 1986.

[12] Uwe Riechert. *Eignung von Polyethylen für Gleichspannungs-Energiekabel*. PhD thesis, Shaker, Aachen, 2002.

[13] Shiliang Zhao, Josef Kindersberger, Maria Hering, and Karsten Juhre. *Influencing factors on field distribution of GIS insulators under DC voltage: 12.-14. November 2018 in Berlin*, volume 157, CD-ROM of *ETG-Fachbericht*. VDE Verlag, Berlin and Offenbach, 2018.

[14] A. Winter, J. Kindersberger, T. Muenchen, M. Tenzer, V. Hinrichsen, T. Darmstadt, L. Zavattoni, O. Lesaint, M. Muhr, Tu Graz, and D. Imamović. Solid/gaseous insulation systems for compact hvdc solutions. *undefined*, 2014.

[15] A. Küchler R. Bärsch. *Beanspruchungen und elektrisches Verhalten von Isoliersystemen bei Gleich- und Mischfeldbeanspruchungen*. Etg-fachtagung, Köln, 28.09.2010.

[16] ING. ANTONINO IMBURGIA. *Modelling of Pulsed Electro Acoustic Method for Space Charge Detection on Single and Multilayer Dielectrics*. Dissertatation, Universita Degli Studi Di Palermo, Palermo, 2018.

[17] Giovanni Mazzanti and Massimo Marzinotto. *Extruded cables for high-voltage direct-current transmission: Advances in research and development*, volume 32 of *IEEE press series on power engineering*. Wiley IEEE Press, Hoboken, 2013.

[18] Ying Li, M. Yasuda, and T. Takada. Pulsed electroacoustic method for measurement of charge accumulation in solid dielectrics. *IEEE Transactions on Dielectrics and Electrical Insulation*, 1(2):188–195, 1994.

[19] Karl Küpfmüller. *Einführung in die theoretische Elektrotechnik*. Deutsche Nationalbibliothek, Leipzig and Frankfurt am Main, 2022.

[20] Thomas Wendel. *Ladungstransport in Epoxidharzformstoff unter Gleichspannungsbelastung*. Dissertation, Shaker and Shaker Verlag, Düren, 2020.

[21] R. Bodega, P.H.F. Morshuis, and J. J. Smit. Space charge measurements on multi-dielectrics by means of the pulsed electroacoustic method. *IEEE Transactions on Dielectrics and Electrical Insulation*, 13(2):272–281, 2006.

[22] Marc Jan Petrus Jeroense. *Charges and discharges in HVDC cables: In particular in mass-impregnated HVDC cables*. Delft University Press, Delft, 1997.

[23] Li Lan, Jiandong Wu, Yi Yin, Xuguang Li, and Zhe Li. Effect of temperature on space charge trapping and conduction in cross-linked polyethylene. *IEEE Transactions on Dielectrics and Electrical Insulation*, 21(4):1784–1791, 2014.